Modeling the Internal Pressure Distribution of a Fuel Cell

Mikko S. Mikkola* and Pauli A. Koski
Helsinki University of Technology TKK, Department of Applied Physics
*Corresponding author: P.O. Box 5100, 02015 TKK, Finland, firstname.lastname@tkk.fi

Abstract: A 3D FEM model for predicting the internal pressure distribution of a fuel cell stack is presented. The model includes contact pair boundary conditions between the most critical components, thermal expansion and Young's moduli as a function of temperature. The model is used to investigate the changes in pressure distribution inside a PEM fuel cell at realistic temperatures from 23 to 160 °C. It was found that increasing temperature made the pressure distribution more uneven. Furthermore, the effect of thermal expansion on pressure distribution was found to be negligible.

Keywords: fuel cell, pressure distribution, modeling, FEM

1. Introduction

A fuel cell stack commonly comprises of planar components which are held together by bolts around the edges. A certain clamping pressure is needed for normal operation, but too high or low pressure can cause various problems. In general, too low pressure leads into reactant leaks, and high electric and thermal contact resistance, while high pressure causes mass transport problems and may damage the components. Furthermore, the clamping pressure is not constant but varies over the cell area. This variation is caused by the flexibility of cell components and location of clamping bolts.

Uneven clamping pressure distribution decreases fuel cell performance and possibly also cell life time by creating uneven current and temperature distributions [1,2,3,4]. Measuring the clamping pressure in situ is highly impractical and ex situ measurements are laborious and usually limited to close to room temperature. Actual fuel cells operate at temperatures between 80 and 1000 °C. Provided that accurate material data is available, an experimentally validated computer model can be used to determine the internal pressure distribution at any temperature and cell geometry.

Some attempts at modeling the pressure distribution inside a polymer electrolyte membrane fuel cell (PEMFC) have been published, e.g. [5,6,7]. Lee et al. [5] modeled the pressure distribution inside a single cell and compared the results to a distribution measured using pressure sensitive films. The trends they observed by measurements and simulation agreed, but there was up to 60% difference between model predictions and measured pressure values. Liu et al. [6] presented an optimization method for the clamping pressure and bolt locations, but their work did not include experimental validation. Karvonen et al. [7] compared various end plate and clamping structures by using a FEM model to predict the pressure distribution inside a fuel cell stack. Their results agreed with the measured distributions qualitatively, but their work did not include quantitative comparison. Mikkola et al. [8] presented a FEM model to simulate the internal pressure distribution of fuel cells, and validated the model by comparing the model predictions against distributions measured from a PEM fuel cell. They used the model to investigate the possibility of using a soft layer between the end plate and other components to equalize the clamping pressure distribution when a less rigid, e.g. non-metallic, end plate is used. However, all the work presented above was carried out at room temperature, and none of the models included thermal expansion or temperature dependent material properties. These are vital factors to consider since the real operating temperature of fuel cells ranges up to 1000 °C.

The model presented here improves on previous work [8] by adding thermal expansion to the model and using material parameters that change as a function of temperature. This allows using the model to predict pressure distributions inside fuel cells under actual operating conditions. Required material parameters are rarely readily available from component manufacturers, and thus some of the parameters had to be determined experimentally.

Internal pressure distributions are presented at various temperatures from 23 up to 160 °C, which is a conceivable operating temperature of a high temperature PEMFC. Various clamping

force arrangements and pressure equalization layers (EQLs), which are proposed to smoothen the pressure distribution are studied using the model. The results are compared against a base case with a basic clamping force scheme and no EQL.

2. Use of COMSOL Multiphysics

2.1 Governing Equations

The model was implemented using COMSOL Multiphysics 3.5 in Solid, Stress-Strain application model. We assumed that linear elasticity applies to all components and solved the displacement field **u** from the equation of motion for a static object

$$\nabla \cdot \left(D \nabla \mathbf{u} \right) = 0 \qquad (1)$$

where D is the elasticity matrix. For isotropic materials D takes the form

$$D = \frac{E}{(1+\nu)(1-2\nu)} \begin{bmatrix} 1-\nu & \nu & \nu & 0 & 0 & 0 \\ \nu & 1-\nu & \nu & 0 & 0 & 0 \\ \nu & \nu & 1-\nu & 0 & 0 & 0 \\ 0 & 0 & 0 & \frac{1}{2}-\nu & 0 & 0 \\ 0 & 0 & 0 & 0 & \frac{1}{2}-\nu & 0 \\ 0 & 0 & 0 & 0 & 0 & \frac{1}{2}-\nu \end{bmatrix} \qquad (2)$$

where E is Young's modulus and ν Poisson's ratio. All relevant stresses and strains can be calculated from the displacement field **u**.

2.2 The Model

Model geometry was fashioned after an existing fuel cell, from which pressure distributions were measured in order to validate the first version of this model [8]. The thin bipolar plate (BPP) substitute used in the pressure distribution measurements was replaced with a graphite one of a more realistic thickness in this model. However, the reactant flow channels, which would be situated on the top surface of the BPP, were left out to simplify the resulting mesh. The model geometry is presented in Figure 1. Only one eighth of the fuel cell had to be modeled due to symmetries. Symmetry planes can also be seen in Figure 1. All other boundaries of the model were free, except for the rings that were drawn and embedded onto the top surface of the end plate, and onto which clamping force from the bolts was applied as a boundary condition.

Contact pair boundary condition was applied between the current collector (CC) and bipolar plate. The contact pair model was not absolutely necessary in this case, since CC and BPP have the same coefficient of thermal expansion and

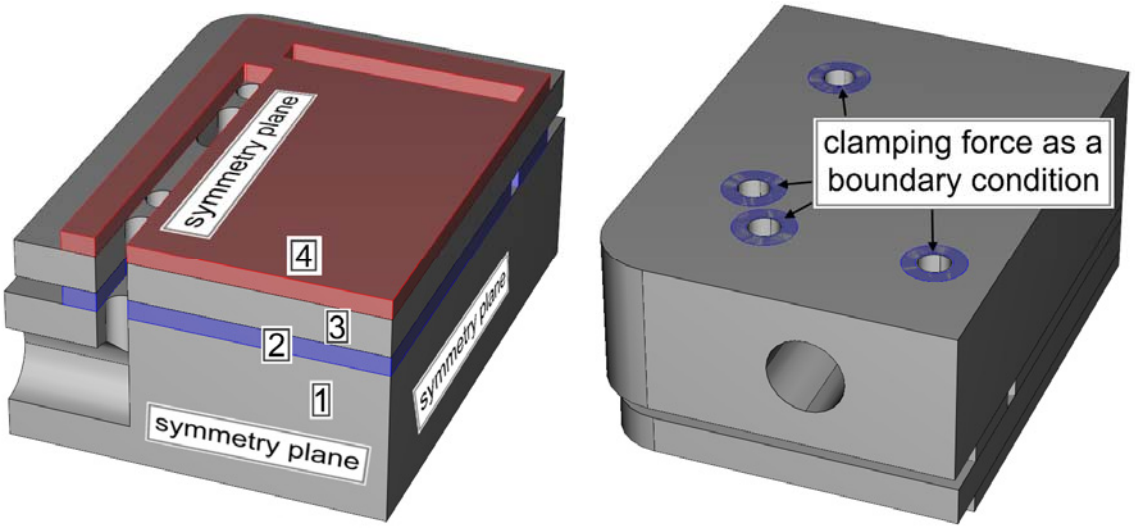

Figure 1. Left: A quarter section along the symmetry planes of one half of the modeled fuel cell. Right: The top side of the end plate. Clamping force was applied onto the marked areas. Cell components: 1) End plate 2) Pressure equalization layer 3) Current collector 4) Bipolar plate. Clamping bolts are not shown in these figures.

will not deform very much. This was done as preparation for future applications of the model, where CC and BPP may not be made of the same material. Contact pairs were not applied between the end plate (EP) and EQL, or EQL and CC, because the EQL is much more pliable than the other components, and due to high friction at the boundaries is less likely to slide than to deform.

2.3 Modeled cases

The primary goal of this work is to study how the temperature dependent material parameters affect the predicted internal pressure distribution. In the previous study [8] the possibility of using an EQL and different clamping force schemes was studied, but the pressure distribution was determined at room temperature. The improved EQL geometry and bolt force scheme were chosen for this study, and the model was solved at room temperature (23 °C), 80, 120 and 160 °C, and the resulting pressure distributions were compared to the room temperature case. For reference, the model was solved also for a case with no EQL and constant clamping force on each bolt, and a case where only thermal expansion was considered. All cases were isothermal. The clamping force scheme and the geometry of the EQL are shown in Figure 2.

2.4 Material parameters

Component materials and parameters used in the model components are given in Table 1. Materials for the end plate and current collector are inherited from the previous version of this model [8]. The BPP substitute in the previous version was replaced with a more realistic version for this study, and the material was changed from PTFE to graphite. Also the EQL material was changed from butyl rubber to a fluoropolymer, since butyl rubber does not tolerate the higher temperatures used in this model.

Temperature dependent material data for the end plate was not available at the time of writing, and thus a constant value was used. For the graphite material and fluoropolymer Young's modulus was measured at several temperatures using an Instron 5567 universal material tester with a Heatwave 240 temperature chamber. The measurement temperatures were 23, 80, 120 and 160 °C.

All materials were assumed isotropic. This is not exactly true for the graphite components, since their thermal and mechanical properties are different for through-plane and in-plane directions. However, this assumption does not cause significant errors, since the model is isothermal and most of the forces act in through-plane direction. Furthermore, coefficients of thermal expansion were assumed constant due to unavailability of reliable data.

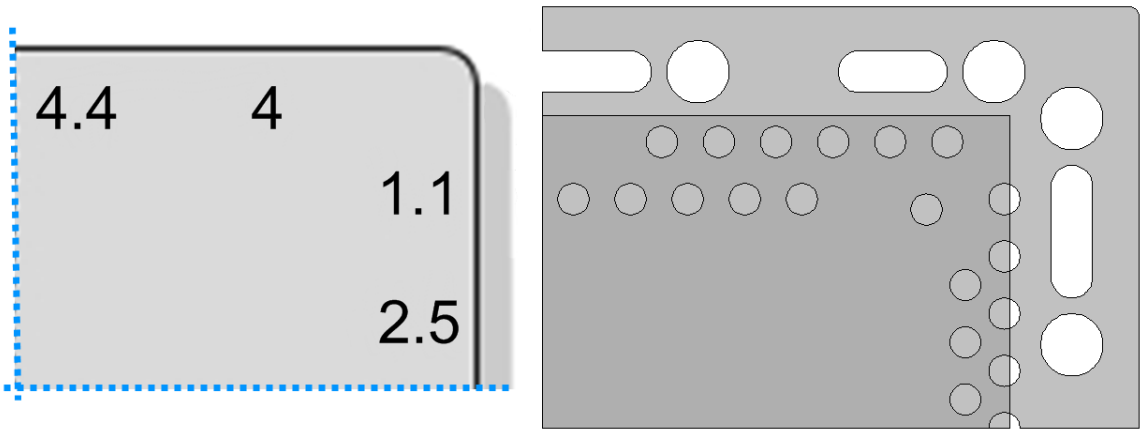

Figure 2. Left: Clamping force per bolt in kN. Right: The shape of the improved EQL from [8]. The darker rectangle indicates the active area of the fuel cell, over which the pressure distribution is the most critical. The dimensions of the active area are 90 mm by 60 mm.

Table 1. List of material parameters for model components

Component	Material	Young's modulus E (MPa)	Poisson's ratio ν	Coefficient of thermal expansion α (1/K)
End plate	PPS + 40% glass fiber	13 000 [9]	0.36 [a]	10^{-5} [9]
EQL	Fluoropolymer rubber	Measured, see Chapter 3.1	0.49 [b]	$16 \cdot 10^{-5}$ [b]
CC & BPP	Graphite	Measured, see Chapter 3.1	0.3 [c]	10^{-5} [d]

[a] Poisson's ratio taken from a material data sheet for a similar product from a different manufacturer [10].
[b] A typical value for common fluoropolymers, see for example [11].
[c] Estimated [d] A typical value for graphite materials, see for example [12].

2.5 Model statistics

A typical version of the model had approximately 200k tetrahedral mesh elements created with the predefined mesh setting 'normal' and ca. 420k degrees of freedom. The model was solved on a server (Intel Core 2 Quad Q9550 with 8 GB of RAM) running COMSOL Multiphysics on 64-bit Linux. Typical solution time was ca. 4 hours for a parametric sweep of four temperature points. For comparison, the model was also solved with a finer mesh for the BPP, where the mesh for the surface boundary of the BPP was created with the mesh setting 'extremely fine'. This increased the number of mesh elements for the BPP from 3.7k to 26.3k, but the resulting pressure distribution was practically identical.

3. Results & Discussion

3.1 Measured Material Parameters

Young's moduli as a function of temperature for the graphite material and fluoropolymer are presented in Table 2. Measurement at each temperature was repeated several times and the standard deviation of the results is used as the limit of error. The graphite material retained its rigidity up to 120 °C, but at 160 °C Young's modulus decreased by ca. 20%. Young's modulus of the fluoropolymer, on the other hand, decreased by ca. 40% already at 80 °C, but remained at that level up to 160 °C. These values were entered into the COMSOL Multiphysics Materials/Coefficients Library and used as material parameters in the model.

Table 2. Measured Young's moduli for the graphite material and fluoropolymer rubber and the calculated change from the room temperature value.

	Graphite		Fluoropolymer	
T (°C)	E (GPa)	Change (%)	E (MPa)	Change (%)
23	2.10 ± 0.05	0	12.96 ± 0.47	0
80	2.16 ± 0.03	2.7	7.89 ± 0.28	-39.1
120	2.08 ± 0.04	-1.3	8.08 ± 0.28	-37.7
160	1.64 ± 0.16	-22.2	8.96 ± 0.27	-30.9

The measured values here are meant to be indicative only and reflect the changes in material parameters as the temperature changes. These data are not meant to be used for engineering purposes.

3.2 The Effect of Temperature Dependent Material Parameters on Pressure Distribution

The predicted internal pressure distributions with the improved EQL and clamping force scheme at 23, 80, 120 and 160 °C are given in Figures 4 to 7 in the Appendix, respectively. Increasing temperature made the temperature distribution over the active cell area more uneven, both increasing the maximum and decreasing the minimum values. The effect can be seen already at 80 °C, indicating that the changes in the properties of the EQL have a visible effect on the internal pressure distribution. This was expected, based on the sensitivity analysis presented in [8]. It was shown that the changes in the EQL properties

alter the pressure distribution more than changes in the properties of the CC. From 120 to 160 °C the change is not very large although the Young's modulus of the CC dropped by 20%. That was probably offset by the small increase in Young's modulus of the EQL that from 120 to 160 °C.

High pressure values on the edges of the bipolar plate in the middle of the horizontal gas manifold result from the structure of the underlying structure. Both the EQL and CC have a solid support under the middle of the manifold and are more resistant to deformation in those areas. That relays more of the clamping force to that area in the BPP, compared to the areas in the middle or end of the manifold. High pressure in the outer corner of the BPP is a consequence of the clamping arrangement, which directs too much of the total force to the corner of the cell.

The EQL and the clamping force scheme were not optimized to produce a uniform pressure distribution over the active area, but they exhibit a clear improvement over the case where there is no EQL and the clamping force at each bolt is constant. Figure 5 shows a pressure distribution for such a case. Most of the clamping force is directed to the outer corner of the cell, where compression pressure is close to 90 bar. Over the active area the pressure is probably too low for good performance and in the middle of the cell the compression pressure is unsubstantial. It has been suggested that the optimum compression pressure for PEMFCs lies between 10 and 20 bar [13].

Internal pressure distributions were calculated at 23, 80, 120 and 160 °C for a case where only thermal expansion was considered, but all material parameters were maintained constant. There were no significant changes between the distributions. This would indicate that thermal expansion does not have a significant effect on the pressure distribution when the temperature changes are smaller than 140 °C.

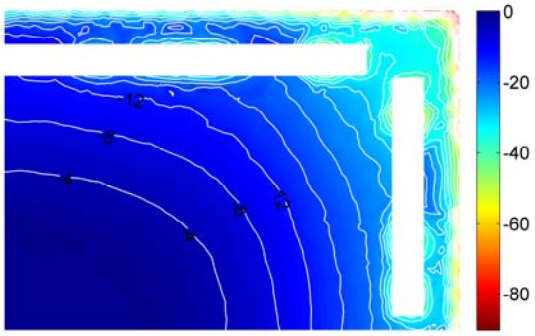

Figure 3. Pressure distribution on the surface of the BPP at 23 °C without an EQL and with constant 3 kN clamping force on each bolt position. Unit: bar.

4. Conclusions

Temperature dependent material parameters were observed to have a significant effect on the internal pressure distribution over the active area of the cell. The distribution became less uniform with increasing temperature. Both the minimum pressure values were decreased and maximum pressure values were increased. The results would imply that it is not sufficient to optimize the compression pressure distribution of the fuel cell stack at the assembly temperature, but the pressure distribution at the real operating temperature should be considered. An experimentally validated computer model can be used for this purpose, as long as reliable material data is available. Determining the compression pressure distribution experimentally is extremely challenging at higher temperatures, while Young's modulus can be readily measured.

Furthermore, it was found that thermal expansion does not play a significant role in low temperature (< 200 °C) fuel cells excluding cases where an assembly or design error places a component in direct contact with e.g. clamping bolt. Expansion against a rigid object may create high internal stresses, which may lead into component deformation or damage.

There are several ways the model presented here can be improved. First, more accurate material data can be used to improve the accuracy of model predictions. Here, Young's modulus of the end plate was assumed constant, although also its rigidity has a significant effect on the resulting internal pressure distribution. Second, in reality the fuel cell stack is not isothermal, but there is a temperature distribution, which depends on the fuel cell type and stack structure. Third, the flow channels on the bipolar plate surfaces and the other components between the bipolar plates, e.g. the electrolyte and gas diffusion layers, should be taken into account. However, the fine detail of these structures causes computational difficulties.

6. References

1. W. Lee, C. Ho, J.W. Van Zee and M. Murthy, *J. Power Sources*, **84**, 45-51 (1999)
2. W. Sun, B.A. Peppley and K. Karan, *J. Power Sources*, **144**, 42–53 (2005)
3. W.R. Chang, J.J. Hwang, F.B. Weng and S.H. Chan, *J. Power Sources*, **166**, 149-154 (2007)
4. I. Nitta, T. Hottinen, O. Himanen and M. Mikkola, *J. Power Sources*, **171**, 26-36 (2007)
5. S. Lee, C. Hsu and C. Huang, *J. Power Sources*, **145**, 353–361 (2005)
6. D. Liu, X. Lai, J. Ni, L. Peng, S. Lan and Z. Lin, *J. Power Sources*, **172**, 760–767 (2007)
7. S. Karvonen, T. Hottinen, J. Ihonen and H. Uusalo, *J. Fuel Cell Sci. Technol.*, **5**, 041009 (2008)
8. Mikko Mikkola, Thomas Tingelöf and Jari K. Ihonen, *J. Power Sources*, **193,** 269-275 (2009)
9. Ensinger Ltd. TECATRON GF 40 data sheet.
10. Dainippon DIC.PPS FZ-2140 data sheet.
11. *Plastic Material Data Sheets*, Published by MatWeb - Division of Automation Creation, Inc., 2004. Electronic ISBN: 978-1-59124-720-3
12. H.O. Pierson, *Handbook of Carbon, Graphite, Diamond and Fullerenes - Properties, Processing and Applications*, Published by William Andrew Publishing/Noyes 1993. Electronic ISBN: 978-0-8155-1739-9
13. Jari Ihonen, Mikko Mikkola, and Göran Lindbergh, *J. Electrochem. Soc.*, **151**, A1152–A1161 (2004)

9. Acknowledgements

This work was carried out under the project "WorkingPEM" funded by TEKES, the Finnish Funding Agency for Technology and Innovation.

10. Appendix - Internal Pressure Distribution Figures

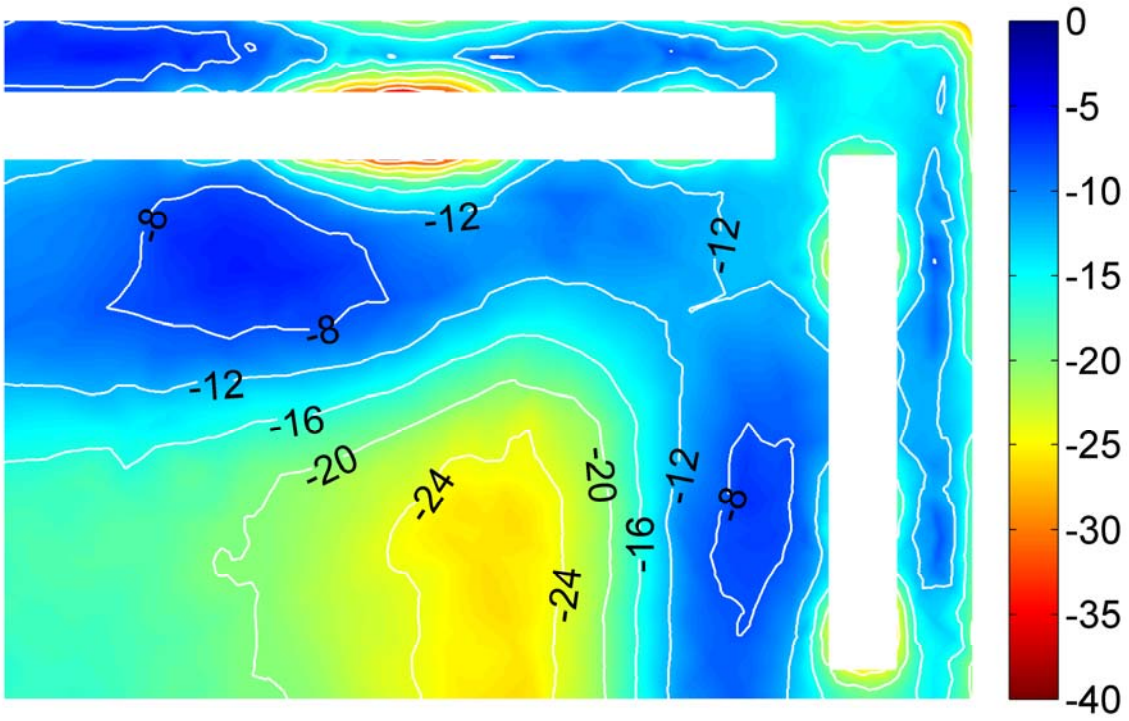

Figure 4. Pressure distribution on the surface of the BPP at 23 °C. Unit: bar.

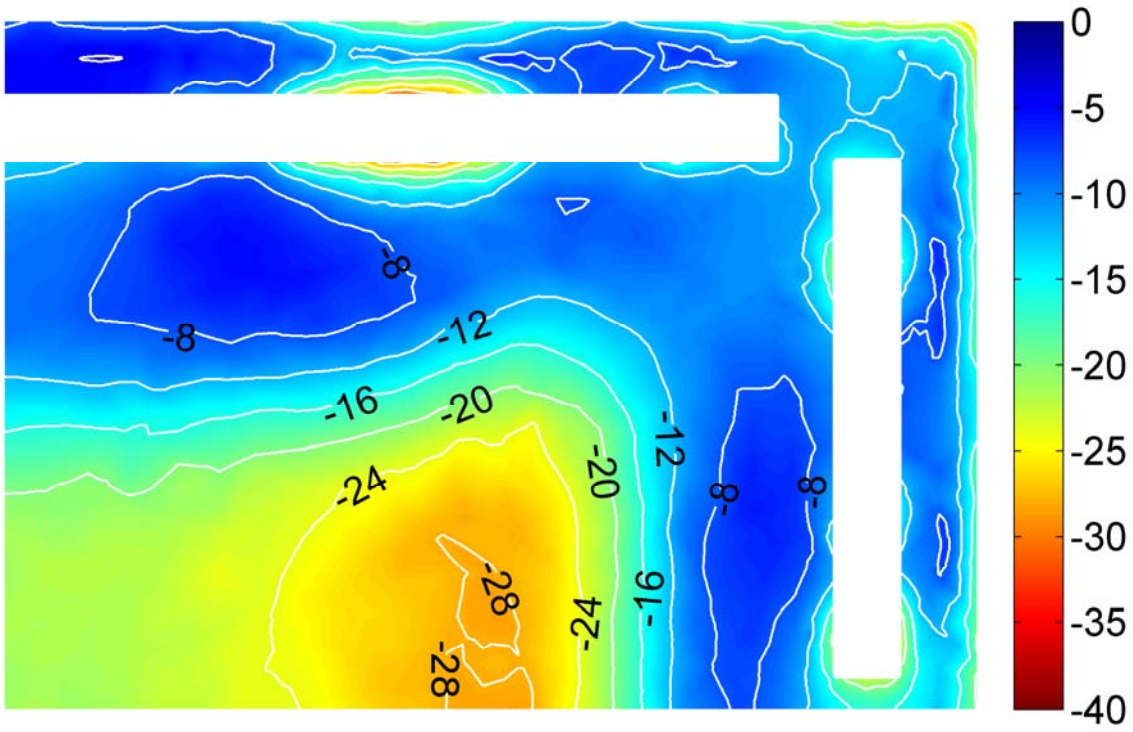

Figure 5. Pressure distribution on the surface of the BPP at 80 °C. Unit: bar.

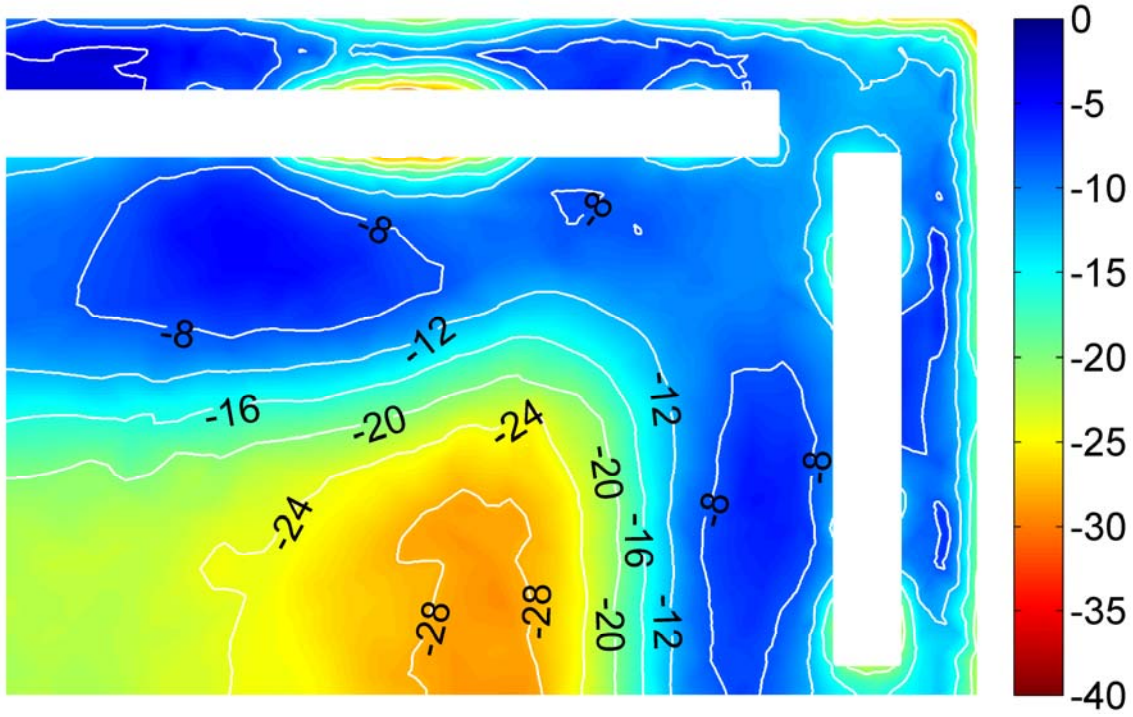

Figure 6. Pressure distribution on the surface of the BPP at 120 °C. Unit: bar.

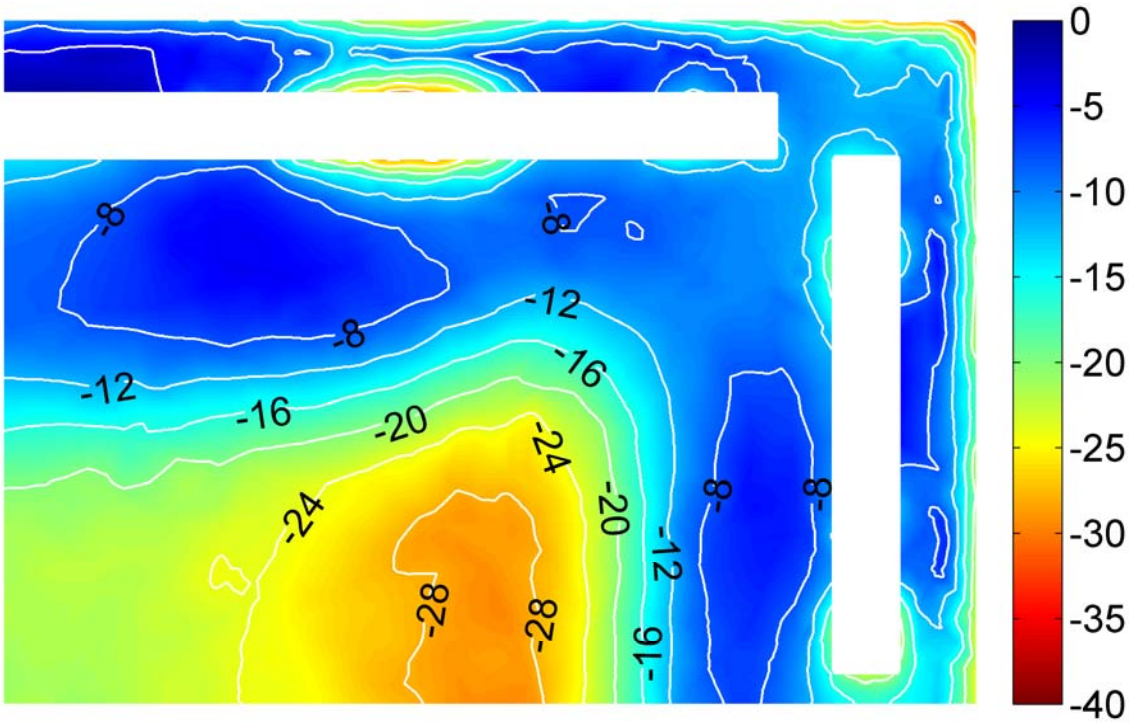

Figure 7. Pressure distribution on the surface of the BPP at 160 °C. Unit: bar.